Supporting information for

Sc^{3+}-triggered oxoiron(IV) formation from O_2 and its nonheme iron(II) precursor via a Sc^{3+}–peroxo–Fe^{3+} intermediate

Feifei Li,[1] Katherine M. Van Heuvelen,[1] Katlyn K. Meier,[2] Eckard Münck,[2,*] and Lawrence Que, Jr.[1]

(1) Department of Chemistry and Center for Metals in Biocatalysis, University of Minnesota, Minneapolis, MN 55455

(2) Department of Chemistry, Carnegie Mellon University, Pittsburgh, PA 15213

1. Materials and Syntheses

All reagents including the TMC ligand, $NaBPh_4$, $Sc(OTf)_3$, HPLC-grade acetonitrile (99.9%) were purchased from commercial sources such as Sigma-Aldrich and Fisher Chemical, and were used as received unless otherwise noted. $[Fe^{II}(TMC)(OTf)](OTf)$ (**1**) was prepared by literature methods in a nitrogen-filled glove-box.[1] $[Fe^{III}(TMC)(\eta^2\text{-}O_2)](OTf)$ was generated by a literature method involving the addition of 10 equiv. NEt_3 and 20 equiv. H_2O_2 to the solution of $[Fe^{II}(TMC)(OTf)](OTf)$ in CH_3CN at –40 ºC.[2]

Oxygenation of 1: CH_3CN solutions of **1** were prepared by dissolving solid **1** in CH_3CN solution under aerobic conditions. To a 1.5 mL CH_3CN solution of 1.0 mM **1** under aerobic conditions, aliquots of both $NaBPh_4$ and $Sc(OTf)_3$ solutions in CH_3CN were injected (e.g. 30 µl of a 50 mM solution of $NaBPh_4$ or $Sc(OTf)_3$ to achieve 1 equiv.) to trigger the formation of **4** in >70% yield, as indicated by its signature absorption bands at 820 nm within 1 h at 0 ºC. Addition of only $NaBPh_4$ or only $Sc(OTf)_3$ to solutions of **1** under aerobic conditions did not alter the UV-visible spectrum of **1** over the same 1-h period at 0 ºC. While the reactant O_2 was provided in the form of air-saturated CH_3CN, the formation of **4** can also occur by bubbling O_2 into CH_3CN solution of **1** under anaerobic conditions in the presence of $NaBPh_4$ and $Sc(OTf)_3$. **4** was the only observed Fe-containing product of this oxygenation reaction of **1** in the presence of $NaBPh_4$ and $Sc(OTf)_3$ in CH_3CN carried between –40 to 25 ºC.

Generation of *purified* $[Fe^{III}(TMC)(\eta^2\text{-}O_2)](BPh_4)$: A 15–20 mM solution of **1** in methanol was prepared by dissolving ~20 mg of this complex in ~1.8 mL MeOH. At –40 ºC, 10 equiv. NEt_3 and 20 equiv. H_2O_2 were added, and the solution was stirred for approximately 15 minutes to allow full formation of $[Fe^{III}(TMC)(\eta^2\text{-}O_2)](OTf)$. The solution was then decanted into a pre-cooled vial containing 5–10 equiv. $NaBPh_4$ and stirred continuously. The blue precipitate of $[Fe^{III}(TMC)(\eta^2\text{-}O_2)](BPh_4)$ formed immediately, and the suspension was stirred for an additional ~60 seconds to make sure that all the solid $NaBPh_4$ had dissolved and the formation of the blue precipitate was complete. The suspension was quickly filtered using a glass-fritted funnel pre-cooled in dry ice to collect the blue precipitate. The precipitate was washed with cold diethyl ether several times. The funnel (containing the blue precipitate) was connected by a rubber adapter to the top of a Schlenk flask, the bottom of which was kept cold with dry ice. Cold CH_3CN (–40 ºC) was then added to the funnel to re-dissolve the precipitate, and vacuum was briefly applied to the Schlenk flask to collect the blue solution into the flask after filtration. The yield of the purified $[Fe^{III}(TMC)(\eta^2\text{-}O_2)](BPh_4)$ complex in the solid state relative to the starting

$[Fe^{III}(TMC)(\eta^2\text{-}O_2)](OTf)$ complex in solution was typically about 60–75%. The blue precipitate of $[Fe^{III}(TMC)(\eta^2\text{-}O_2)](BPh_4)$ was re-dissolved in cold CH_3CN at –40 ˚C to make a stock solution of 1.0–1.5 mM with its concentration based on ε_{835} = 650 $M^{-1}cm^{-1}$. The blue precipitate of $[Fe^{III}(TMC)(\eta^2\text{-}O_2)](BPh_4)$ prepared in this manner was fairly stable under anaerobic conditions as long as it was kept at –40 ºC. In contrast, if precipitated out from CH_3CN rather than MeOH, the blue precipitate of $[Fe^{III}(TMC)(\eta^2\text{-}O_2)](BPh_4)$ decomposed into a yellowish material shortly after precipitation, even at low temperatures. This protocol thus enables the isolation of purified $[Fe^{III}(TMC)(\eta^2\text{-}O_2)](BPh_4)$ in a form that is not contaminated by excess NEt_3 or H_2O_2.

Sc^{3+} adduct of $[Fe^{III}(TMC)(\eta^2\text{-}O_2)]^+$ (3): **3** can be generated by two methods with method A starting with $[Fe^{III}(TMC)(\eta^2\text{-}O_2)](OTf)$ generated in solution *and* method B using re-dissolved $[Fe^{III}(TMC)(\eta^2\text{-}O_2)](BPh_4)$. **Method A**: after the generation of $[Fe^{III}(TMC)(\eta^2\text{-}O_2)](OTf)$ in CH_3CN from 10 equiv. NEt_3 and 20 equiv. H_2O_2 (e.g. 1.5 mM) at –40 ºC,[2] addition of >10 equiv. $Sc(OTf)_3$ afforded **3** instantly with the absorption band shifting from 835 nm to 520 nm in the UV-visible spectra. While **3** prepared by this method was fairly stable at –40 ºC, addition of <10 equiv. Sc^{3+} resulted in an unstable form of **3** that quickly decayed to a purple species within a minute. **Method B**: addition of ≥1.0 equiv. $Sc(OTf)_3$ to a solution of $[Fe^{III}(TMC)(\eta^2\text{-}O_2)](BPh_4)$ (see last paragraph for details) immediately generated **3**. Preparations of **3** generated by these two methods exhibited identical UV-visible features, EPR signals, and Mössbauer parameters (using ^{57}Fe-enriched precursors). Resonance Raman studies of **3** were conducted on samples prepared from Method A for economical purposes; titration and decay reactions were monitored with **3** prepared by Method B to prevent possible complications from NEt_3 and H_2O_2.

Oxygenation reactions of **1** were followed by monitoring the increase in absorbance at 820 nm in UV-visible spectra due to the formation of $[Fe^{IV}(O)(TMC)]^{2+}$ (**4**). Yields of **4** were determined by its absorbance at 820 nm (ε_{820} = 400 $M^{-1}cm^{-1}$).[1]

For the identification and quantification of the decay product of BPh_4^-, the same reactions were carried out in CD_3CN at 0 ºC in the presence of 1 equiv. $NaBPh_4$ and 1 equiv. $Sc(OTf)_3$ followed by running the product solution through a mini-column filled with basic alumina to remove iron complexes. The ^{1}H NMR spectrum of the resulting colorless solution afforded a set of resonances that matched very well with the standard spectra of biphenyl. An internal standard (either 2,6-dimethyl-4-methoxy-phenol or 2,4,6-trimethyl-phenol) was then added to quantify the

concentrations of biphenyl. The internal standards were purified according to published procedures.[3]

2 Physical methods.

UV-Vis spectra were recorded on a HP8453A diode-array spectrometer equipped with a cryostat from Unisoku Scientific Instruments (Osaka, Japan) for temperature control. X-band EPR spectra were obtained at liquid helium temperatures (4K) on a Bruker Elexsys E-500 spectrometer equipped with an Oxford ESR-910 cryostat. ^{1}H NMR was collected on a Varian Inova 300 MHz spectrometer at room temperature. Electrospray ionization mass spectrometry (ESI-MS) studies were conducted on a Bruker BioTof II instrument under positive ion mode with a typical *m*/*Z* range of 100 – 1250. Mössbauer spectra were recorded with two spectrometers, using Janis Research Super-Varitemp dewars that allowed studies in applied magnetic fields up to 8.0 T in the temperature range from 1.5 to 200 K. Mössbauer spectral simulations were performed using the WMOSS software package v2.5 (WEB Research, Edina, MN).

We have analyzed the Mössbauer spectra of **3** with the Hamiltonian of equation 1.

$$\mathcal{H} = D\left(S_z^2 - \frac{35}{4}\right) + E(S_x^2 - S_y^2) + g_0\beta \boldsymbol{S}\cdot\boldsymbol{B} + \boldsymbol{S}\cdot\boldsymbol{A}\cdot\boldsymbol{I} - g_n\beta_n \boldsymbol{B}\cdot\boldsymbol{I} + \mathcal{H}_Q \quad \textbf{(1)}$$

where *D* and *E* are the axial and rhombic ZFS parameters, *A* is the ^{57}Fe magnetic hyperfine tensor and $\mathcal{H}_Q$ describes the nuclear quadrupole interactions:

$$\mathcal{H}_Q = \frac{eQV_{zz}}{12}\left[3I_z^2 - I(I+1) + \eta\left(I_x^2 - I_y^2\right)\right] \quad \textbf{(2)}$$

where e is the proton charge, V_{zz} is an element of the electric field gradient tensor, and η is the asymmetry parameter.[2]

Resonance Raman spectra were collected on an ACTON AM-506M3 monochromator with a Princeton LN/CCD data collection system (LN-1100PB) using a Spectra Physics Model 2060 krypton laser or a Spectra Physics Beamlok 2065-7S argon laser, and Kaiser Optical holographic super-notch filters. Low-temperature spectra of **3** in CH_3CN were obtained at 77 K using a 135° backscattering geometry. Samples were frozen onto a gold-plated copper cold finger in thermal contact with a Dewar flask containing liquid nitrogen. The Raman frequencies were referenced to indene. Slits were set for a band-pass of 4 cm^{-1} for all spectra. Raman spectra were baseline corrected, and intensity corrected according to the 773 cm^{-1} solvent peak of CH_3CN.

Fe K-edge X-ray absorption spectroscopic studies of **3** were conducted at beamline X3B of the National Synchrotron Light Source (NSLS) at the Brookhaven National Lab in Upton, NY. The sample consisted of a 4.3 mM solution of **3** frozen in acetonitrile in a large tandem Mössbauer/XAS sample cup. The sample was run in fluorescence mode using a new 31 element Canberra Ge detector. The sample was maintained at ~ 19 K during data collection. In order to prevent possible photoreduction, data were collected on three different spots on a single sample. Three scans were collected on the first spot, and two additional scans were collected on each of two additional spots. The raw XAS data were examined, average, and processed for analysis with EXAFSPAK.[4] No channels were excluded from the analysis. No points were excluded from the raw data. Due to noise in the data at high k values, deglitching was performed at k~11.7, 13.4, and 13.7 by fitting the EXAFS data with a cubic function in EXAFSPAK, which allowed us to consider a k range of 2-14 $Å^{-1}$ (resolution = 0.132 Å). To confirm that deglitching did not influence the fit, both the "raw" data and the deglitched data were fit with the same parameters. Fits were generated using the opt program in EXAFSPAK. The energies were referenced against an internal Fe foil reference at 7112.0 eV. A unit-weighted average was used for both data sets. The $k^3\chi(k)$ EXAFS data was analyzed using EXAFSPAK with phase and amplitude parameters derived from FEFF 8.40.[5] The goodness-of-fit parameter F is defined as $[\Sigma k^6(\chi_{expt} - \chi_{calc})^2 / \Sigma k^6(\chi_{expt})^2]^{1/2}$. A second goodness-of-fit parameter F' is defined as $F' = F^2 / \nu$, where $\nu = N_{IDP} - \rho$. N_{IDP} is the number of independent data points ($N_{IDP} = 2\Delta k \Delta r/\pi$), and ρ is the number of floated variables in each optimization step.[6] F' is a measure of whether an added shell significantly improves the fit. In all analyses, the coordination number of a given shell was kept as a fixed parameter, and varied iteratively when bond lengths, Debye-waller factors, and the edge shift parameter E_0 were allowed to freely float. The scale factor S_0 was set to 0.9

X-ray Absorption Near Edge Structure (XANES) data **3** were taken on a frozen solution sample (~4.3 mM in CH_3CN) at beamline 7-3 of Stanford Synchrotron Radiation Lightsource (SLAC National Accelerator Laboratory, Menlo Park, CA). Pre-edge analysis of **2** and **5** were carried out for XAS data that were also collected at 7-3 beamline of SSRL, with the corresponding sample descriptions and XAS analyses previously published.[2] The data were collected in fluorescence mode using a 30-element germanium detector (Canberra) at a sample temperature of *ca.* 10 K. The pre-edge region was curve-fitted using SSExafs to generate pre-edge areas according to published protocols.[7,8] The heights, positions, and widths of preedge peaks were refined using a Gaussian function and all parameters were allowed to float freely for the final fit.

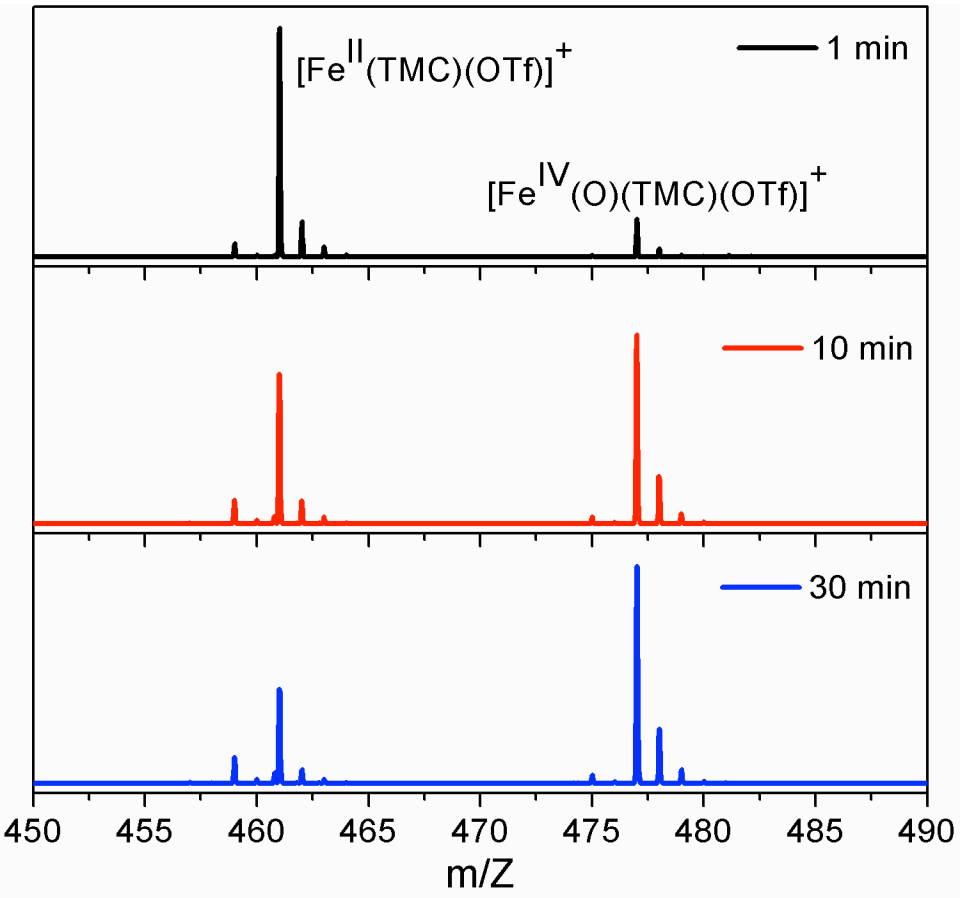

Figure S1. Electrospray ionization (ESI) mass spectra for the reactions of $[Fe^{II}(TMC)(NCCH_3)](OTf)_2$ with $O_2/Sc(OTf)_3/NaBPh_4$ in CH_3CN at 25 ºC. Small aliquots of the solution were collected at 1-min, 10-min, and 30-min time-points after the reaction was initiated and injected into an ESI mass spectrometer in positive ion mode.

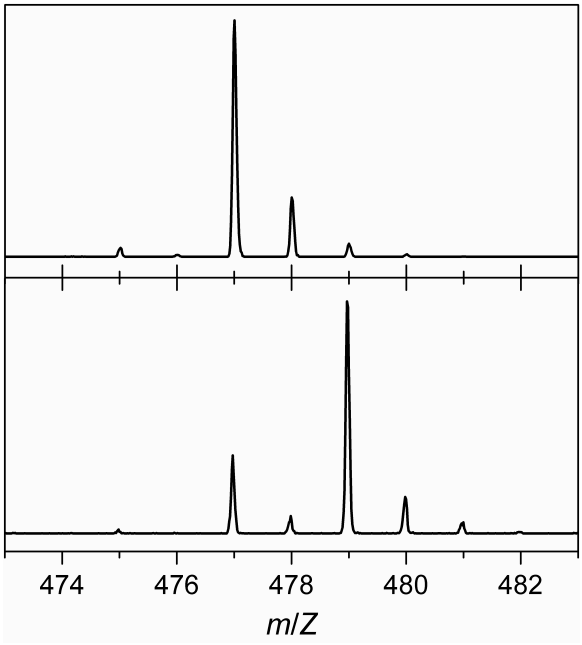

Figure S2. Electrospray ionization mass spectra of $\{[Fe^{IV}(O)(TMC)](OTf)\}^{+}$ prepared from acetonitrile solution of **1**, Sc^{3+}, BPh_4^-, and O_2 ($^{16}O_2$ in the top panel:and$^{18}O_2$ in the bottom panel).

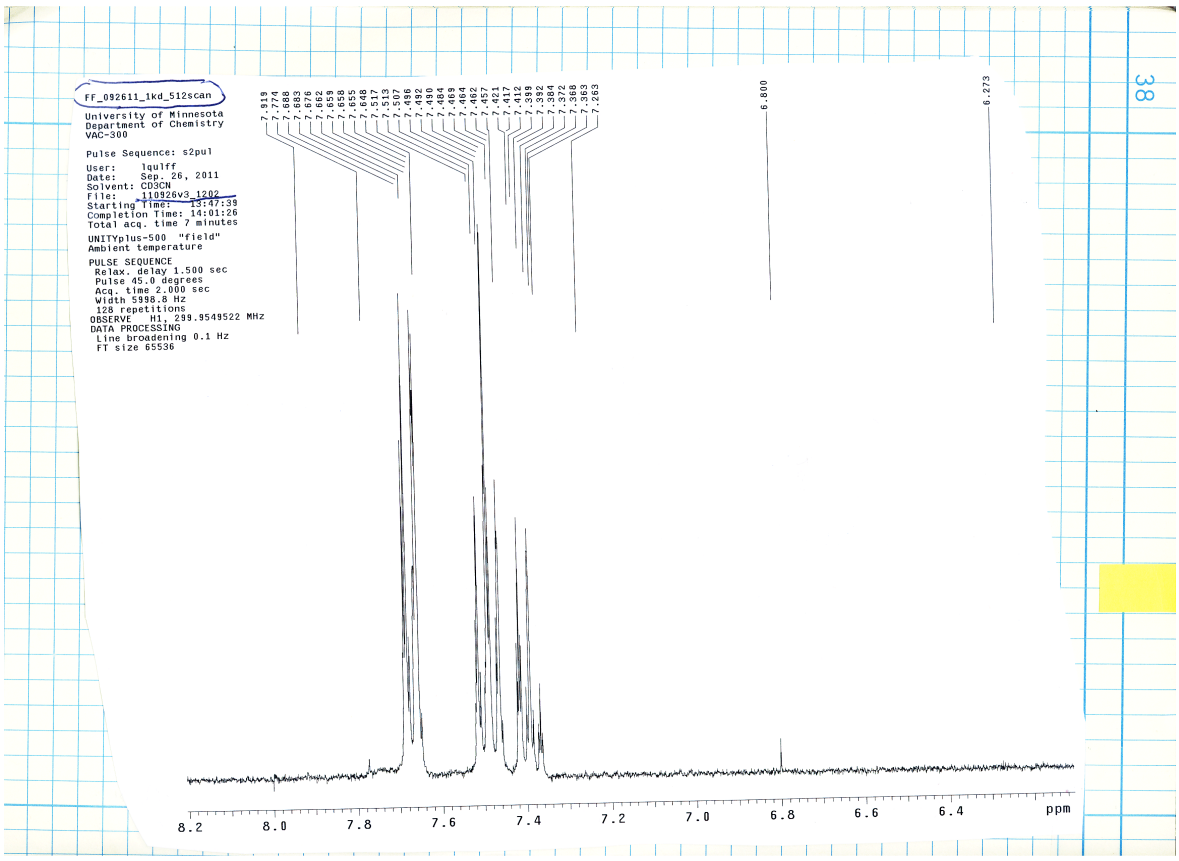

Figure S3. ^{1}H NMR spectrum of organic products in CD_3CN generated from the oxygenation reaction of **1** in the presence of 1 equiv. $Sc(OTf)_3$ and 1 equiv. $NaBPh_4$ (reaction temperature is 0 ºC) followed by filtering out any iron complexes by a flash column of alumina (basic). Only peaks derived from 1,1'-biphenyl were observed in the ^{1}H NMR spectrum.

3. XAS analysis and results.

As shown in Figure S4 and listed in Table S1, the first inflection point of the Fe K-edge occurs at 7125.3 eV, which was taken as the edge energy. In comparison, $[Fe^{III}(O_2)(TMC)]^+$ (**2**) and $[Fe^{III}(OOH)(TMC)]^{2+}$ (**5**) both had an edge energy of 7125.1 eV.

Table S1. Pre-edge analysis of **2**, **3**, and **5**.

	E_0 (eV)	$E_{pre\text{-}edge}$ (eV)	Height	Width	Area*
2	7125.1	7113.5	0.057(2)	2.13(10)	12.9 (7)
		7115.4	0.022(2)	2.13 (10)	5.0 (4)
3	7125.3	7113.3	0.056(2)	2.40(10)	14.4(6)
5	7125.1	7114.1	0.076(1)	2.78(5)	22.4(4)

*Pre-edge areas have been multiplied by a factor of 100.

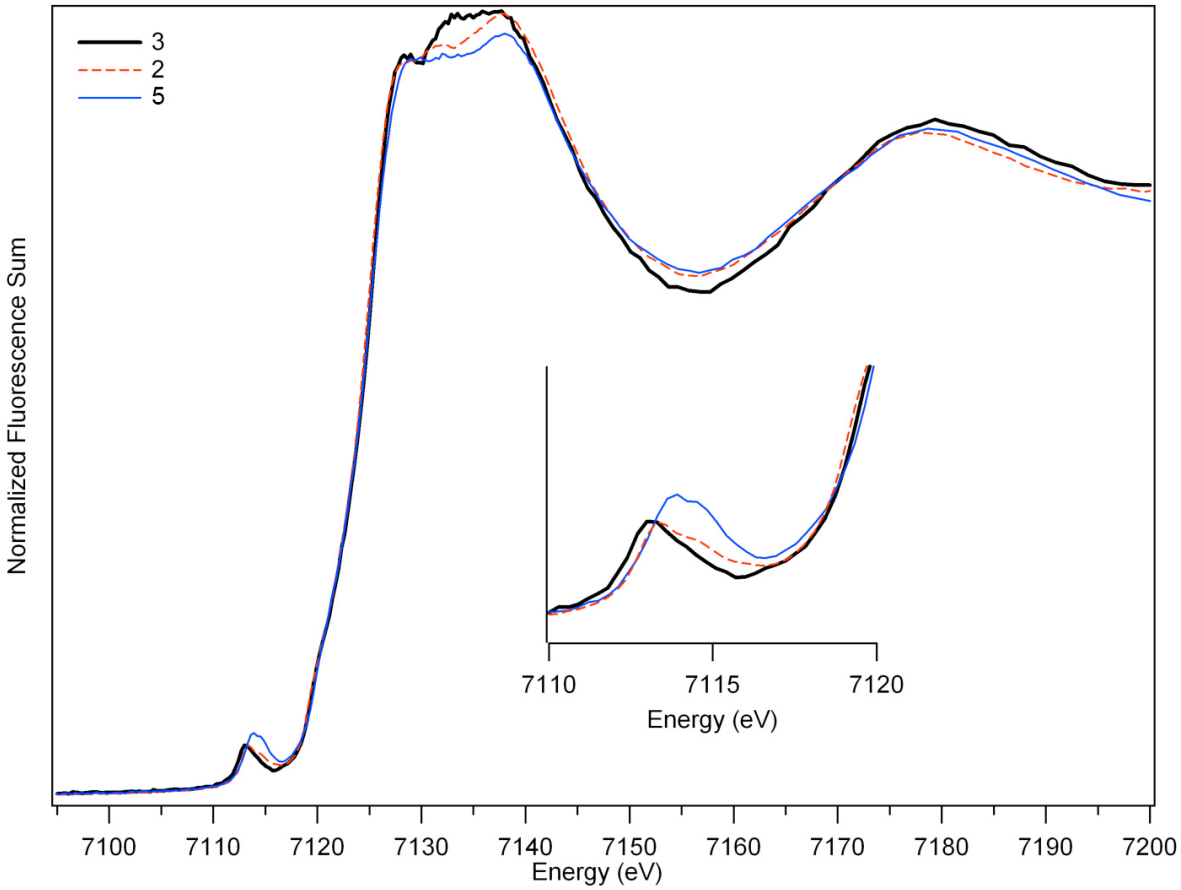

Figure S4. Fe *K*-edge XANES spectra for **2** (red dashed line), **3** (black solid line), and **5** (blue solid line).

The best fits of the EXAFS data corresponding to **3** include four N/O scatterers at ~2.18 Å that are assigned to the TMC macrocycle. Increasing the coordination number to five yielded an unreasonably large σ^2 value of ~12 (Fit 3 in Table S2) and suggests the axial site *trans* to the peroxo moiety is vacant. The overall quality of fits, as measured by the goodness-of-fit parameter F and the edge shift (E_0), is greatly improved by the addition of a second shell at ~1.98 Å, which is derived from peroxo ligand (Fits 4 and 5 in Table S2). The inclusion of a single O/N scatterer at ~1.98 Å (Fit 4) produces an unreasonable σ^2 value of less than 0. On the other hand, the inclusion of two such scatterers (Fit 5) produces a reasonable σ^2 value of ~3 that is comparable to that found for **2**, indicating that the peroxo ligand coordinated in a symmetric side-on (η^2) fashion. Carbon scatterers attributed to the TMC ligand are apparent at ~2.99 and 3.15 Å, reminiscent of EXAFS fits of $[Fe^{III}(O_2)(TMC)]^+$ and $[Fe^{III}(OOH)(TMC)]^{2+}$.[2]

We also attempted to include a scandium scatterer in the EXAFS model. A slight improvement in GOF (fits 13 and 14 in Table S2) was obtained with the inclusion of a Sc scatterer of 3.8 Å that has a reasonable Debye-Waller factor in the unfiltered data set ($\sigma^2 \sim 4$). Such an Fe•••Sc distance can be compared with the Fe•••Cu distance of 3.6-3.7 Å found for a Cu(μ-η^2:η^2-peroxo)heme complex by EXAFS and DFT.[9] However, the following two considerations prevented us from unambiguously identifying the Sc scatterer. First, inclusion of the Sc scatterer only marginally improves the F-factor, probably due to the low intensity of distant scatterers in the outer shell; Second, different Fe•••Sc distances yielded comparable values of F and E_0. For example, while the best fit placed the Sc^{3+} scatterer at ~3.82 Å from the iron center, moving the heavy atom to ~4.09 Å produced a fit of comparable quality (Table S2, fits 14 and 15). Therefore, we conclude that the Sc scatterer could not be definitively located in the EXAFS analysis. It is not surprising that the effect of the Sc scatterer is not more pronounced because that scandium is not a particularly heavy scatterer and distant scatterers in the Fourier-transformed spectrum typically result in low intensity unless fixed by strong interactions. Moreover, the dynamic vibrational disorder experienced by **3** could lead to different Fe•••Sc distances. Similarly, EXAFS analysis of $[Co^{IV}(O)(TMG_3tren)(ScOTf_3)]^{2+}$ (recently reformulated as $[Co^{III}(OH)(TMG_3tren)(ScOTf_3)]^{2+}$ by Borovik[10]) also did not reveal a scandium scatterer.[11]

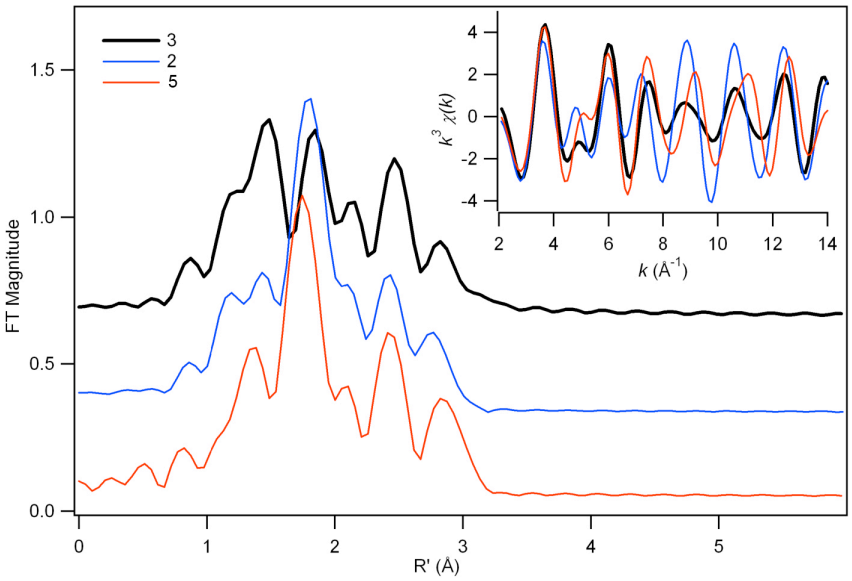

Figure S5. Fourier transform of Fe *K*-edge EXAFS data for **3** (black line, offset 0.65), **2** (blue line, offset 0.40), and **5** (red line, offset 0.00) over a *k*-range of 2-14 Å^{-1} with $k^3\chi(k)$ vs *k* data shown in the inset. Back-transform range: 0.3 to 3.0 Å (**2**), 0.75 to 3.2 Å (**3**), and 0.3–3.2 Å^{-1} (**5**).

References

(1) Rohde, J.-U.; In, J.-H.; Lim, M. H.; Brennessel, W. W.; Bukowski, M. R.; Stubna, A.; Münck, E.; Nam, W.; Que, L., Jr. *Science* **2003**, *299*, 1037-1039.
(2) Li, F.; Meier, K. K.; Cranswick, M. A.; Chakrabarti, M.; Van Heuvelen, K. M.; Munck, E.; Que, L. *J. Am. Chem. Soc.* **2011**, *133*, 7256-7259.
(3) Armarego, W. L. F.; Perrin, D. D. *Purification of Laboratory Chemicals*; Butterworth-Heinemann: Oxford, 1997.
(4) George, G. N.; Pickering, I. J.; Stanford Synchrotron Radiation Laboratory, Stanford Linear Accelerator Center: Stanford, California, 2000.
(5) Ankudinov, A. L. R., B.; Rehr, J. J.; Conradson, S. D. *Phys. Rev. B: Condens. Matter Mater. Phys.* **1998**, *58*, 7565–7576.
(6) Riggs-Gelasco, P. J.; Stemmler, T. L.; Penner-Hahn, J. E. *Coord. Chem. Rev.* **1995**, *144*, 245-286.
(7) Scarrow, R. C.; Trimitsis, M. G.; Buck, C. P.; Grove, G. N.; Cowling, R. A.; Nelson, M. J. *Biochemistry* **1994**, *33*, 15023-15035.
(8) Shan, X.; Rohde, J.-U.; Koehntop, K. D.; Zhou, Y.; Bukowski, M. R.; Costas, M.; Fujisawa, K.; Que, L., Jr. *Inorg. Chem.* **2007**, *46*, 8410-8417.
(9) Halime, Z.; Kieber-Emmons, M. T.; Qayyum, M. F.; Mondal, B.; Gandhi, T.; Puiu, S. C.; Chufán, E. E.; Sarjeant, A. A. N.; Hodgson, K. O.; Hedman, B.; Solomon, E. I.; Karlin, K. D. *Inorg. Chem.* **2010**, *49*, 3629-3645.
(10) Lacy, D. C.; Park, Y. J.; Ziller, J. W.; Yano, J.; Borovik, A. S. *J. Am. Chem. Soc.* **2012**, *134*, 17526-17535.
(11) Pfaff, F. F.; Kundu, S.; Risch, M.; Pandian, S.; Heims, F.; Pryjomska-Ray, I.; Haack, P.; Metzinger, R.; Bill, E.; Dau, H.; Comba, P.; Ray, K. *Angew. Chem. Int. Ed.* **2011**, *50*, 1711-1715.

Table S2. EXAFS fitting results for **3**, considering the unfiltered data, $k = 2 – 14$ Å (resolution 0.132 Å).

	Fe–N/O			Fe–O/N			Fe•••Sc			Fe•••C			Fe•••C					
Fit	*N*	r (Å)	σ $^{2(a)}$	*N*	r (Å)	σ ^{2}	*N*	r (Å)	σ ^{2}	*N*	r (Å)	σ ^{2}	*N*	r (Å)	σ ^{2}	E_0	F	F’
1	3	2.20	5.07													8.05	447.8	785.8
2	4	2.20	8.12													5.95	431.7	771.5
3	5	2.17	12.88													4.20	423.1	763.8
4	4	2.18	4.31	1	1.98	-0.40										2.23	246.9	583.5
5	4	2.19	3.22	2	1.98	2.83										0.55	250.8	588.1
6	4	2.19	3.19	2	1.98	2.76				4	3.11	6.58				0.10	181.4	500.1
7	**4**	**2.18**	**3.57**	**2**	**1.98**	**2.85**				**4**	**3.00**	**2.25**	**4**	**3.15**	**1.10**	**-1.30**	**141.30**	**441.5**
8	5	2.17	6.50	1	1.96	-0.40				4	3.02	2.33	4	3.16	1.13	-0.33	149.50	454.1
9	4	2.18	3.94	2	1.98	3.17	1	3.26	0.47	4	2.99	-1.30	4	3.12	-3.00	-1.33	123.80	413.2
10	4	2.19	3.24	2	1.98	2.80	1	3.15	7.92							0.15	207.30	534.7
11	4	2.19	3.21	2	1.98	2.86	1	3.82	6.24							0.67	246.80	583.4
12	4	2.19	3.19	2	1.98	2.77	1	3.82	6.26	4	3.11	6.55				0.20	177.90	495.2
13	4	2.18	3.61	2	1.98	2.92	1	3.82	4.36	4	3.00	1.95	4	3.15	0.77	-1.19	136.60	433.9
14	4	2.18	3.60	2	1.98	2.90	1	3.82	4.60	4	3.00	1.98	5	3.15	1.85	-1.27	134.40	430.5
15	4	2.18	3.61	2	1.98	2.87	1	4.10	4.13	4	3.00	2.05	5	3.15	2.04	-1.40	134.10	430.1

F = goodness of fit parameter = $[\Sigma^6(\chi_{expt} - \chi_{calc})^2 / \Sigma k^6(\chi_{expt})^2]^{1/2}$

F’ = weighted F factor = F^2 / ν, where $\nu = N_{IDP} - \rho$. N_{IDP} is the number of independent data points ($N_{IDP} = 2\Delta k \Delta r/\pi$), and ρ is the number of floated variables in each optimization step

Table S3. EXAFS fitting results for **3**, considering the deglitched, unfiltered data, $k = 2 – 14$ Å (resolution 0.132 Å).

	Fe–N/O			Fe–O/N			Fe•••Sc			Fe•••C			Fe•••C				
Fit	*N*	r (Å)	$\sigma^{2(a)}$	*N*	r (Å)	σ^2	*N*	r (Å)	σ^2	*N*	r (Å)	σ^2	*N*	r (Å)	σ^2	E_0	F
16	3	2.21	4.60													7.47	358.1
17	4	2.19	8.97													5.60	356.1
18	5	2.17	13.05													4.11	344.7
19	4	2.18	4.79	1	1.97	-0.10										2.00	196.1
20	4	2.19	3.64	2	1.98	3.20										0.30	199.4
21	4	2.19	3.62	2	1.98	3.11				4	3.10	6.46				-0.21	128.7
22	**4**	**2.18**	**3.78**	**2**	**1.98**	**3.08**				**4**	**3.02**	**3.36**	**4**	**3.16**	**2.40**	**-1.17**	**95.91**
23	4	2.19	3.65	2	1.98	3.10	1	3.14	7.93							-0.26	155.10
24	4	2.18	3.74	2	1.97	2.90	1	3.20	3.60	4	3.03	3.41				-1.43	104.20
25	4	2.18	3.99	2	1.98	3.12	1	3.25	0.24	4	2.98	-0.50	4	3.11	-2.60	-1.64	82.89
26	4	2.19	3.62	2	1.98	3.19	1	3.80	6.64							0.37	195.50
27	4	2.19	3.59	2	1.98	3.09	1	3.80	6.62	4	3.10	6.41				-0.13	125.20
28	4	2.18	3.79	2	1.98	3.09	1	3.81	6.07	4	3.01	3.29	4	3.16	2.24	-1.13	92.58
29	4	2.18	3.79	2	1.97	3.08	1	3.80	6.13	4	3.00	3.32	5	3.15	3.24	-1.24	89.97

Table S4. EXAFS fitting results for **3**, considering the filtered data, $k = 2 – 14$ Å (resolution 0.132 Å) with a back-transform range of 0.75 to 3.2 Å.

	Fe–N/O			Fe–O/N			Fe•••Sc			Fe•••C			Fe•••C				
Fit	*N*	r (Å)	$\sigma^{2(a)}$	*N*	r (Å)	σ^2	*N*	r (Å)	σ^2	*N*	r (Å)	σ^2	*N*	r (Å)	σ^2	E_0	F
30	4	2.20	8.19													6.48	157.3
31	4	2.18	4.64	1	1.97	0.00										2.00	74.62
32	4	2.19	3.55	2	1.98	3.12										-0.11	76.99
33	4	2.19	3.50	2	1.98	3.13				4	3.10	7.22				-0.17	36.79
34	4	2.18	3.83	2	1.97	3.18				4	3.01	1.51	4	3.16	0.62	-1.33	8.23
35	**4**	**2.18**	**3.83**	**2**	**1.97**	**3.14**				**4**	**3.00**	**1.38**	**5**	**3.15**	**1.61**	**-1.46**	**6.88**
36	4	2.18	3.87	2	1.97	3.18	1	3.83	26.07	4	3.00	1.46	5	3.15	1.69	-1.43	6.50